Emission source functions in heavy ion collisions

V. M. Shapoval,[1] Yu. M. Sinyukov,[1,*] and Iu. A. Karpenko[1,2]

[1]*Bogolyubov Institute for Theoretical Physics, Metrolohichna Street 14b, 03680 Kiev, Ukraine*

[2]*Frankfurt Institute for Advanced Studies, Ruth-Moufang-Straße 1, 60438 Frankfurt am Main, Germany*

(Received 29 August 2013; revised manuscript received 11 October 2013; published 5 December 2013)

Three-dimensional pion and kaon emission source functions are extracted from hydrokinetic model (HKM) simulations of central Au + Au collisions at the top Relativistic Heavy Ion Collider (RHIC) energy $\sqrt{s_{NN}} =$ 200 GeV. The model describes well the experimental data, previously obtained by the PHENIX and STAR collaborations using the imaging technique. In particular, the HKM reproduces the non-Gaussian heavy tails of the source function in the pair transverse momentum (*out*) and beam (*long*) directions, observed in the pion case and practically absent for kaons. The role of rescatterings and long-lived resonance decays in forming the mentioned long-range tails is investigated. The particle rescattering contribution to the *out* tail seems to be dominating. The model calculations also show substantial relative emission times between pions (with mean value 13 fm/c in the longitudinally comoving system), including those coming from resonance decays and rescatterings. A prediction is made for the source functions in Large Hadron Collider (LHC) Pb + Pb collisions at $\sqrt{s_{NN}} = 2.76$ TeV, which are still not extracted from the measured correlation functions.

DOI: 10.1103/PhysRevC.88.064904 PACS number(s): 25.75.Gz, 24.10.Nz

I. INTRODUCTION

The common method for accessing spatio-temporal characteristics of expanding superdense systems formed in ultrarelativistic heavy-ion collisions is the correlation interferometry (or correlation femtoscopy) technique [1–3]. It is based on the connection between the size and shape of the region where the particles are produced (from the one side), and the form of the corresponding two-particle relative momentum distribution (from another side). Physically this connection originates from the quantum statistics effect of symmetrization (antisymmetrization) of the two-particle wave function, leading to the enchancement (suppression) of the production of particles with close momenta. Femtoscopic analysis utilizes the experimentally measured two-particle momentum correlation function, which is constructed as the ratio of the actual particle-pair distribution over the relative momentum (where pairs are formed by the particles from the same event) to the analogous distribution of the pairs of particles from mixed events. This correlation function is typically fitted with a certain analytical expression. In most cases its quantum statistical component[1] is supposed to be Gaussian $1 + \lambda e^{-\sum_i q_i^2 R_i^2}$, but in the general case it depends on the researcher's assumptions about the emission function, thus being model dependent. The correlation function fit gives one the interferometry radii R_i, commonly interpreted as the i-direction system's homogeneity lengths [6,7]. It allows one to estimate the important characteristics of the dynamics of heavy ion collisions, such as the lifetime of the fireball created, gradients of the collective velocities, duration of emission, etc.

In some sense a complementary method of obtaining information about the space-time structure of the system from the correlation measurements is known as source imaging [8–10]. It is based on the extraction of the time-integrated distribution of the relative distance between particle radiation points in the pair rest frame (PRF) from the measured correlation function. In contrast to the standard approach, allowing us to determine only the interferometry radii which are interpreted then in the previously assumed model, source imaging reveals the actual non-Gaussian source function, being in this sense model independent. Then, once the source function is obtained, one can readily fit it with different model expressions and extract the corresponding parameters. Having the source function, apart from the Gaussian interferometry radii, one will also know the detailed source structure, which can likely deviate from the Gaussian distribution, having a more complicated shape. This fact can be caused by different reasons, such as collision geometry, long-lived resonance contribution [11–13], space-momentum correlations due to either collective motion [14,15] or string fragmentation [16], etc. The source imaging in combination with collision model simulations gives the possibility to study the influence of these effects on the source form. Another advantage of the imaging technique is that, in contrast to the correlation function, the source function reflects the properties of the emission region itself, refined from the final state interaction (FSI) and quantum statistics (QS) effects.

In Ref. [17] the authors investigate the source breakup dynamics in Au + Au collisions at $\sqrt{s_{NN}} = 200$ GeV, analyzing two-pion source functions extracted from the experimental data. They observed a specific power-law tail in the pair-momentum and beam direction source function projections, interpreted as evidence for the noticeable emission duration time and long time delays between emissions from different points of the source, in particular because of long-lived resonance decays. The kaon source function, obtained in the STAR Collaboration Au + Au collision experiment at a similar energy [18] does not contain an analogous heavy tail, that

*Corresponding author: sinyukov@bitp.kiev.ua

[1]Usually one supposes that contributions of the quantum statistical, the final state interaction, and the non-femtoscopic correlations to the full correlation function can be separately accounted for in the fit [4,5].

 ©2013 American Physical Society

probably indicates a lesser role of the resonance's halo in the kaon emission and its almost instantaneous nature.

The tails observed in the pion source function can be interesting also in view of the activity devoted to the search of the phase transition between the quark-gluon plasma (QGP) and the hadron gas, which could be expected to take place during the evolution of systems produced in ultrarelativistic nuclear collisions [19]. The idea of such studies is that, due to the soft equation of state (leading to the speed of sound $c_s = (\frac{\partial p}{\partial \epsilon})_s^{1/2}$ close to zero, $c_s \approx 0$), which the system has at the first-order phase transition, its expansion should slow down and the lifetime should increase. The source function's non-Gaussian tails can be considered as the possible signal of such prolonged system lifetime.

To detail the interpretation of the extracted experimental data, one usually compares them with the results of calculations in different event generators, such as THERMINATOR [20] or hadronic rescattering calculations [21] (HRC). Based on such comparisons, one can see certain peculiarities of the system evolution. Another way of using the model source functions is by including them into the correlation function fitting expressions, which account for the FSI effects, such as the Lednický and Lyuboshitz analytical model [22]. Such models are utilized to fit the experimental data and extract the parameters characterizing the interaction between particles, such as scattering lengths, effective radii, etc. This method allows one to find out the characteristics of, e.g., strong interaction between particles of exotic species, which can hardly be measured in ordinary scattering experiments, but are accessible for the FSI correlation technique in relativistic heavy-ion collisions (see, e.g., [23]). The analytical approximations to the correlation function depend on both the source and the interaction characteristics, that complicates the interpretation of the experimental data, increasing the number of free parameters in the fitting expression. Calculating the parameters that describe the source separately in the event generator simulations could facilitate and improve the reliability of the interaction analysis.

However, each of the mentioned models lacks completeness in the description of the matter evolution process and involves a set of substantial simplifications. This complicates the analysis of the physical reasons of observed effects and most probably leads to missing some features of the explored phenomena. For example, in most THERMINATOR calculations the simple blast-wave [24] parametrization for the freeze-out hypersurface and flow is used, and particle rescatterings are not implemented. The HRC includes rescattering treatment, but accounts only for eight types of resonance decays and assumes kinematic evolution of particles just from the time $t = 0$ fm/c, at which the simple parametrization for the initial particle momenta and coordinate distributions is exploited.

In this paper we present an analysis of the source functions calculated in the hydrokinetic model (HKM) [25–27], exactly, in its hybrid version (hHKM). The latter includes a pure hydrodynamic stage, passing on to the hydrokinetic one, describing the gradual liberation of particles from an expanding fluid, which is then switched on a spacelike hypersurface to the UrQMD hadronic cascade. Thus, the model provides a realistic description of the full process of evolution of the matter produced in relativistic nuclear collisions and is known to successfully describe a wide class of various observables [28]. The simulations were performed to describe the results for 20% most central Au + Au collisions at $\sqrt{s_{NN}} = 200$ GeV at the Relativistic Heavy Ion Collider (RHIC) and to make a prediction for 5% most central Large Hadron Collider (LHC) Pb + Pb collisions at $\sqrt{s_{NN}} = 2.76$ TeV.

In Sec. II we briefly discuss the physical meaning of the emission source function and describe the idea of the source imaging technique. In Sec. III we show the results of our calculations, compare them with experimental data, and give our interpretation. In Sec. IV we summarize our results and make concluding remarks.

II. SOURCE FUNCTION AND SOURCE IMAGING METHOD

As follows from the previous section, the emission source function is an important object used in the analysis of the space-time structure of nuclear collisions. In theoretical studies based on computer simulations one can easily extract the simulated source function directly from the event generator output, as we do in the present article. However, in experiments one needs to utilize the source imaging technique to extract the source function from the measured correlation function $C(p, q)$. To make the relation of the source function to the experimental observables more clear, in this section we remind the reader of definition of the source function and the basic ideas of the source imaging method.

Analyzing experimental data, the researcher aims to extract from it all possible information about the explored object. Studying particle emission in a relativistic nucleus-nucleus collision one would like to know the emission function $g(x, p) = \frac{d^7N}{d^4x d^3p}$: the distribution of the emitted particles over the space-time coordinates and momentum components, which would provide exhaustive information about the analyzed process. However, in practice it turns out that the maximum possible knowledge about this process, obtainable in typical experiments where the single-, two-, and even many-particle momentum spectra are measured, is limited, so that $g(x, p)$ and even the less informative Wigner function $f_W(x, p) = \frac{d^6N}{d^3x d^3p}$ cannot be reconstructed in a model-independent way [29].

To see this, one can write the following expression for the Wigner phase-space density function $f_W(x, p)$ [30]:

$$f_W(x, p) = (2\pi)^{-3} \int d^4q \, \delta(q \cdot p) e^{-iqx} \langle a^\dagger_{p-q/2} a_{p+q/2} \rangle, \quad (1)$$

justified for the case of weakly interacting particles. Here $a^\dagger_k$, a_k are the creation and annihilation operators of particles with momentum k, $q = p_1 - p_2$, $p = \frac{p_1+p_2}{2}$, and p_1, p_2 are the particle momenta. The delta function $\delta(q \cdot p)$ under the integral sign corresponds to the assumed mass-shell constraint, and the brackets $\langle \cdots \rangle$ mean averaging over the density matrix associated with the spacelike hypersurfaces, at which particles become almost free (for sudden freeze-out the thermal density matrix at the freeze-out hypersurface can be used).

One can see that, to restore the Wigner function, one should have the possibility to extract the quantity $\langle a^\dagger_{p-q/2} a_{p+q/2}\rangle$. But can it be done, based on common experimental data? Typically in the experiment one measures the single-particle $W(p)$ and the two-particle $W(p_1, p_2)$ momentum spectra to construct the two-particle correlation function

$$C(p_1, p_2) = \frac{W(p_1, p_2)}{W(p_1)W(p_2)}. \tag{2}$$

The spectra can be expressed through $a^\dagger_p$ and a_p,

$$\begin{aligned} W(p) &= E\frac{d^3N}{d^3p} = \langle a^\dagger_p a_p\rangle, \\ W(p_1, p_2) &= E_1E_2\frac{d^6N}{d^3p_1 d^3p_2} = \left\langle a^\dagger_{p_1} a^\dagger_{p_2} a_{p_2} a_{p_1}\right\rangle \\ &= W(p_1)W(p_2) + \left|\left\langle a^\dagger_{p_1} a_{p_2}\right\rangle\right|^2, \end{aligned}$$

where it is supposed that the four-operator average $\langle a^\dagger_{p_1} a^\dagger_{p_2} a_{p_2} a_{p_1}\rangle$ can be decomposed into the sum of products of two-operator ones,

$$\left\langle a^\dagger_{p_1} a^\dagger_{p_2} a_{p_2} a_{p_1}\right\rangle = \left\langle a^\dagger_{p_1} a_{p_1}\right\rangle\left\langle a^\dagger_{p_2} a_{p_2}\right\rangle + \left\langle a^\dagger_{p_1} a_{p_2}\right\rangle\left\langle a^\dagger_{p_2} a_{p_1}\right\rangle. \tag{4}$$

From the Eq. (3) it follows that, having measured single- and two-particle momentum spectra, one can determine only the absolute value of $\langle a^\dagger_{p-q/2} a_{p+q/2}\rangle$, so it will be known only to the phase factor.[2] This information is surely insufficient to restore the Wigner function (1).

The emission function $g(x, p)$ is connected with the Wigner function through the integral equation [below $x_0 \equiv (t_{\sigma_0}(\mathbf{x}_0), \mathbf{x}_0 = \mathbf{x} + (\mathbf{p}/p_0)[t_{\sigma_0}(\mathbf{x}_0) - t])$ corresponds to the portion of the system, which propagates without collisions until some time t starting from the initial hypersurface σ_0, $x' \equiv (t', \mathbf{x} + (\mathbf{p}/p_0)(t' - t))$]

$$f_W(x, p) = f_W(x_0, p) + p^0\int_{t_0}^{t} dt' g(x', p), \tag{5}$$

so its reconstruction makes the task even harder. That is why the analysis of the space-time structure of the emission process has to be performed in terms of other (less informative) characteristics. The source function $S(\mathbf{r}^*)$ is one of them. It is usually defined as a time-integrated pair separation distribution in the pair rest frame.

In the experiment $S(\mathbf{r}^*)$ is restored from the measured correlation function $C(p, q)$. To figure out the connection between $S(\mathbf{r}^*)$ and $C(p, q)$, one can express both of them via the emission function $g(x, p)$. If the smoothness approximation is assumed, the spectra (3) can be written as

$$\begin{aligned} W(p) &= p^0\int d^4x\, g(x, p), \\ W(p_1, p_2) &\approx p_1^0 p_2^0\int d^4x_1 d^4x_2 g_1(x_1, p_1) g_2(x_2, p_2)|\psi(\tilde{q}, r)|^2, \end{aligned} \tag{6}$$

where $\psi(\tilde{q}, r)$ is a reduced Bethe-Salpeter amplitude corresponding to the relative motion of the particles making the pair with the generalized relative four-momentum $\tilde{q} = q - p(q\cdot p)/p^2$ and separation r. For the case of identical particles it should be replaced by the (anti)symmetrized amplitude, $\psi(\tilde{q}, r) \to [\psi(q, r) \pm \psi(-q, r)]/\sqrt{2}$. Here one supposes also that the two-particle emission function is defined only by two-particle interaction, whereas other effects such as many-body interactions or event-wide correlations are neglected.

After substitution of (6) into (2) the correlation function reads as

$$\begin{aligned} &C(p, q) \\ &\quad = 1 + \frac{\int d^4x_1 d^4x_2 g_1(x_1, p_1) g_2(x_2, p_2)(|\psi(\tilde{q}, r)|^2 - 1)}{\int d^4x_1 g_1(x_1, p_1)\int d^4x_2 g_2(x_2, p_2)}. \end{aligned} \tag{7}$$

Then one can introduce the relative distance distribution function $s(r, p_1, p_2)$ as the convolution of normalized emission functions,

$$\begin{aligned} s(r, p_1, p_2) &= \frac{\int d^4R g_1(R + r/2, p_1) g_2(R - r/2, p_2)}{\int d^4R g_1(R, p_1)\int d^4R g_2(R, p_2)} \\ &= \int d^4R \tilde{g}_1(R + r/2, p_1)\tilde{g}_2(R - r/2, p_2), \end{aligned} \tag{8}$$

where a tilde denotes the normalized emission function, $R = \frac{x_1+x_2}{2}$, and $r = x_1 - x_2$.

The femtoscopic correlations take place mainly between the particles with small relative particle velocities, $v_1 \approx v_2$. At this approximation for a pair with total momentum $P = p_1 + p_2$ one has [22] $p_1 \approx \frac{m_1}{m_1+m_2}P$ and $p_2 \approx \frac{m_2}{m_1+m_2}P$ in (8), so that $s(r, p_1, p_2)$ does not depend on q. Assuming also the on-shell approximation, $P^0 = \sqrt{(m_1 + m_2)^2 + \mathbf{P}^2}$, one obtains

$$\begin{aligned} s(r, \mathbf{P}) = \int d^4R\, \tilde{g}_1\left(R + r/2, \frac{m_1}{m_1 + m_2}\mathbf{P}\right) \\ \times \tilde{g}_2\left(R - r/2, \frac{m_2}{m_1 + m_2}\mathbf{P}\right). \end{aligned} \tag{9}$$

In the pair rest frame, which we mark by an asterisk—where $\tilde{q} = \{0, \mathbf{q}^*\}$, $\mathbf{P}^* = 0$, and supposing the equal-time approximation to be justified, $t^* = t_1^* - t_2^* = 0$, in the argument of $\psi(\tilde{q}, r)$—one can substitute the Bethe-Salpeter amplitude in (7) by the stationary solution of the scattering problem $\psi(\mathbf{q}^*, \mathbf{r}^*)$. Such a substitution is valid provided that the condition [22] $|t^*| \ll m_{2,1}r^{*2}$ for $\mathrm{sgn}(t^*) = \pm 1$ respectively is fulfilled. This is usually true for heavy particles such as kaons or protons. For pions produced in typical nuclear collisions, the equal-time approximation leads to a slight overestimation (<5%) of the strong FSI effect and it does not influence the leading zero-distance ($r^* \ll |a|$, a being the pair Bohr radius)

[2]It can be shown that the same situation takes place even if one includes many-particle spectra into consideration.

effect of the Coulomb FSI [22,31]. Then one can connect the correlation function with the time-integrated $s(r^*, \mathbf{P}^*)$, obtaining the so-called Koonin equation [22,31–36],

$$\begin{aligned} R(\mathbf{q}^*, \mathbf{0}) &= C(\mathbf{q}^*, \mathbf{0}) - 1 \\ &= \int d^3r^* \int dt^* s(r^*, \mathbf{0})[|\psi(\mathbf{r}^*, \mathbf{q}^*)|^2 - 1] \\ &= \int d^3r^* S(\mathbf{r}^*) K(\mathbf{r}^*, \mathbf{q}^*). \end{aligned} \tag{10}$$

where the function $K(\mathbf{r}^*, \mathbf{q}^*)$ represents the kernel of the integral transform and $S(\mathbf{r}^*) = \int dt^* s(r^*, \mathbf{0})$ is the source function. The latter is interpreted as the probability density of emission of two particles at the relative distance **r*** in their rest frame. Thus, it is normalized to unity,

$$\int d^3r^* S(\mathbf{r}^*) = 1. \tag{11}$$

Extraction of $S(\mathbf{r}^*)$ from the correlation function (7) requires inverting the integral relation (10). This operation is the central problem of imaging. It appears that computationally it is easier to reduce this three-dimensional problem to the series of one-dimensional ones. Such simplification can be achieved using the expansion of $R(\mathbf{q}^*)$, $S(\mathbf{r}^*)$, and $K(\mathbf{r}^*, \mathbf{q}^*)$ in terms of spherical $Y_{lm}(\Omega)$ or Cartesian $A_{\mathbf{l}}(\Omega)$ harmonics:

$$Y_{lm}(\Omega) = \sqrt{\frac{2l+1}{4\pi}\frac{(l-m)!}{(l+m)!}} P_l^m(\cos\theta) e^{im\phi}, \tag{12}$$

where $P_l^m(\cos\theta)$ are associated Legendre polynomials, $l = 0, 1, 2, \ldots$ and $m = -l, \ldots, l$;

$$\begin{aligned} A_{\mathbf{l}}(\Omega) = \sum_{m_i=0}^{l_i/2} &\left(-\frac{1}{2}\right)^m \frac{(2l-2m-1)!!}{(2l-1)!!} \frac{l_x!}{(l_x-2m_x)!m_x!} \\ &\times \frac{l_y!}{(l_y-2m_y)!m_y!} \frac{l_z!}{(l_z-2m_z)!m_z!} \\ &\times n_x^{l_x-2m_x} n_y^{l_y-2m_y} n_z^{l_z-2m_z}. \end{aligned} \tag{13}$$

Here $\mathbf{n} = \{n_x, n_y, n_z\}$ is a unit vector in the Ω direction, $l_x + l_y + l_z = l$, $m_x + m_y + m_z = m$, and $(-1)!! = 1$. Cartesian harmonics $A_{\mathbf{l}}(\Omega)$ are linear combinations of spherical harmonics $Y_{lm}(\Omega)$ corresponding to one l and different m.

The function decomposition in, for example, spherical harmonics looks like

$$\begin{aligned} R(\mathbf{q}^*) &= \sqrt{4\pi} \sum_{lm} R_{lm}^*(q^*) Y_{lm}(\Omega_{\mathbf{q}^*}), \\ S(\mathbf{r}^*) &= \sqrt{4\pi} \sum_{lm} S_{lm}^*(r^*) Y_{lm}(\Omega_{\mathbf{r}^*}), \\ K(\mathbf{q}^*, \mathbf{r}^*) &= 4\pi \sum_{lm} K_l(q^*, r^*) Y_{lm}(\Omega_{\mathbf{q}^*}) Y_{lm}^*(\Omega_{\mathbf{r}^*}), \end{aligned} \tag{14}$$

where $R_{lm}(q^*) = \frac{1}{\sqrt{4\pi}} \int d\Omega_{\mathbf{q}^*} Y_{lm}(\Omega_{\mathbf{q}^*}) R(\mathbf{q}^*)$ and $S_{lm}(r^*) = \frac{1}{\sqrt{4\pi}} \int d\Omega_{\mathbf{r}^*} Y_{lm}(\Omega_{\mathbf{r}^*}) S(\mathbf{r}^*)$ are called spherical *correlation* and *source* moments respectively. Here and below in this section q^*, r^* mean magnitudes of the corresponding three-vectors. Substitution of the obtained expansions (14) into Eq. (10) gives one the series of one-dimensional integral equations with respect to source function spherical moments $S_{lm}(r^*)$:

$$R_{lm}(q^*) = 4\pi \int dr^* r^{*2} S_{lm}(r^*) K_l(q^*, r^*). \tag{15}$$

Apart from simplifying imaging calculations, the decomposition of the correlation function in harmonics, in contrast to its one-dimensional projections, represents complete information about the three-dimensional correlation structure and provides focused insight into the specific physical properties of the emission process (see, e.g., [37]).

For instance, the R_{00} moment represents angle-integrated correlation, being sensitive mainly to the invariant radius R_{inv}. The moments corresponding to $l = 1$ provide access to "Lednicky offset" [38], telling us which sort of particles was emitted earlier. They vanish in the case of identical particles due to symmetry. R_{20} is sensitive to the ratio of transversal and longitudinal source sizes. The more it differs from zero, the stronger is the asymmetry that takes place between these sizes. The moment R_{22} corresponds to the outward-to-sideward system size ratio. As for the moments with $l = 3$, they contain information about the so-called boomerang triaxial deformation and also disappear for identical particles. The moments with $l \geqslant 4$ provide rather detailed information about the source and are not intensively studied at the moment. Also, the harmonic decomposition is more directly connected with the source shape [39] and simplifies the analysis of non-femtoscopic correlations [40].

As for solving the system (15), in the most simple cases, when the analyzed correlation function contains information only about the quantum statistics correlations, it can be performed analytically using the inverse integral transform. In this case the kernel moments $K_l(q^*, r^*)$, containing spherical Bessel functions j_l, define the Fourier-Bessel transform, which can be easily inverted using the completeness relation for j_l,

$$S_{lm}(r^*) = 4\pi \int_0^\infty dq^* q^{*2} K_l^{-1}(q^*, r^*) R_{lm}(q^*), \tag{16}$$

where $K_l^{-1}(q^*, r^*)$ is the inverse transform kernel. But in the general case, when the kernel $K(\mathbf{q}^*, \mathbf{r}^*)$ is more complicated, $K_l^{-1}(q^*, r^*)$ cannot be found in an analytical form. Instead of finding it, one can discretize Eq. (15) and solve it numerically:

$$\begin{aligned} R_{lm}(q_i) &= 4\pi \sum_j \Delta r r_j^2 S_{lm}(r_j) K_l(q_i, r_j) \\ &= \sum_j K_{ij}^l S_j^{lm}, \end{aligned} \tag{17}$$

where $i = 1, \ldots, N_q$, $j = 1, \ldots, N_r$ with N_q and N_r being the numbers of discrete points where the values of $R_{lm}(q^*)$ and $S_{lm}(r^*)$ are specified. Since generally $N_q \neq N_r$, the obtained system of linear equations can be under- or overdetermined. So, one usually tries to find the values S_j (for each l, m) using the method of χ^2minimization:

$$\chi^2 = \sum_i \frac{\left(\sum_j K_{ij} S_j - R_i\right)^2}{\sigma_i^2} \tag{18}$$

with σ^2 being the variance of observed correlation moments R_{lm}. Equating the χ^2 derivative with respect to S_j to zero, one

obtains the following series of equations:

$$\sum_{ij} \frac{1}{\sigma_i^2}(K_{ij}S_j - R_i)K_{ij} = 0. \quad (19)$$

Its solution in matrix form is [8]

$$S = (K^T K)^{-1} K^T R. \quad (20)$$

However, the integral equation (15) that has to be solved is a homogeneous Fredholm integral equation, which is actually an ill-posed problem for numerical solution because of the singular or ill-conditioned K matrix. Singularity in the context of numerical calculations means that the matrix has one or more eigenvalues negligibly small as compared to the others. It leads to instability of the resulting solution, i.e., small uncertainties in the R_i values can cause big uncertainties in S_j. Thus, the solution will not be a smooth function and will be different depending on the solving algorithm. This problem is quite general and is well known for the whole inverse problem class. There are certain methods that can be applied to increase the solution stability [9], but their successful application, resulting in an unambiguous imaging problem solution, i.e., extracting the source function from the experimental data, is a nontrivial and complicated task.

Fortunately, to obtain the model source function from the event generator one does not need to utilize the imaging technique, since in this case the source function can be extracted from the program output straightforwardly. The next section contains the results of a source function calculation in the hydrokinetic model, its interpretation, and comparison with experiment.

III. RESULTS AND DISCUSSION

The hydrokinetic model [25–27] simulates the evolution of matter formed in the relativistic heavy-ion collisions. The full process is supposed to pass in two stages: a continuous medium expansion, described in the ideal hydrodynamics approximation, which then goes over to gradual system decoupling, described in the hydrokinetic approach. At the first stage matter is supposed to be in local chemical and thermal equilibrium. Here we use the lattice-QCD inspired equation of state for the quark-gluon phase [41], matched via a crossover-type transition with the hadron resonance gas, consisting of all 329 well established hadron states made of u, d, and s quarks. As the system expands and cools down, it reaches the second stage, supposed to begin at the chemical freeze-out isotherm $T_{\rm ch} = 165$ MeV. At temperatures $T < T_{\rm ch}$ the system gradually loses both chemical and thermal equilibrium, and the particles begin to continuously escape from the medium. In the hybrid model version (hHKM) the hydrokinetic description of the second stage is switched to an ultrarelativistic quantum molecular dynamics (UrQMD) hadron cascade on a spacelike hypersurface, situated behind the hadronization one. Another option consists of direct switching to the cascade just from the hydrodynamics, at the hadronization hypersurface $T_{\rm ch} = 165$ MeV. We use this particular variant in the current analysis, relying on the result of [28], where the comparison of one- and two-particle spectra, calculated at both types of matching hydrodynamic and cascade stages, showed a quite small difference between them in the considered case of top RHIC and LHC energies. The reason for the similarity is that for the utilized event-averaged initial conditions the contribution from the negative number of the particles crossing nonspacelike sectors of the matching hydro-UrQMD hypersurface is quite small, ~1–2 percent. This is because of very high hydrodynamic velocities ($0.7c$) of the fluid elements crossing nonspacelike parts of the chemical freeze-out isotherm. Then the number of the particles that move inside the fluid belongs to a tail of the relativistic (Boltzmann) spectra and their negative contributions in the Cooper-Frye formula are negligible.

At the switching hypersurface a set of particles is generated according to the corresponding distribution function using either the Cooper-Frye prescription [42] (for sudden switching from hydrodynamics to UrQMD) or the technique of Boltzmann equations in integral form [26,27] (if hydrokinetics is involved). This set serves as input for UrQMD, which performs particle rescatterings and decays. The final model output is again a collection of particles, characterized by their momenta and the points of their last collision.

HKM showed itself to be successful in a simultaneous description of kaon and pion femtoscopy together with corresponding momentum spectra at top RHIC and LHC energies [27,28]. So we can expect the source functions extracted from the model also to be realistic and reliable. Here we present the pion and kaon source functions generated by HKM using parameters adjusted for description of the data from the RHIC 20% most central Au + Au collisions at $\sqrt{s_{NN}} = 200$ GeV. Also the predictions concerning the LHC 5% most central Pb + Pb collisions at $\sqrt{s_{NN}} = 2.76$ TeV are demonstrated.

We work in the central rapidity slice and assume longitudinal boost invariance. Early thermalization at proper time $\tau = 0.1$ fm/c is supposed. In the transverse plane we use a Glauber Monte Carlo (MC) initial energy density profile generated by the GLISSANDO code [43]. The fluctuations of initial conditions tilt in each event the principal axes of the ellipse of inertia and shift the center of mass relative to the reaction-plane coordinate system. To account for this effect, we superpose the principal axes by rotation and recentering of each initial distribution, and after that take averages over the ensemble of events (so-called variable geometry analysis, also implemented as an option in GLISSANDO). So we use event-averaged initial conditions. Also we suppose small but nonzero initial transverse flow which is taken to be linear in the transverse radius r_T [28]: $y_T = \alpha \frac{r_T}{R^2(\phi)}$. Here $R(\phi)$ is a system's homogeneity length in the ϕ direction; we take it as the r.m.s. $R(\phi) = \sqrt{\langle r^2 \rangle_\phi}$ along an azimuthal angle ϕ. Such a small initial flow mimics the shear viscosity effects at the system evolution based on perfect hydrodynamics as well as the effects of event-by-event fluctuating hydrodynamics solutions [28]. Maximal initial energy density ϵ_0 is chosen to reproduce the experimental mean charged particle multiplicity. Thus, ϵ_0 and the coefficient α are the only fitting parameters of the model. For the case of Au + Au collisions at $\sqrt{s_{NN}} = 200$ GeV we take the parameters from [28] corresponding to the best fit for the pion, kaon, and proton spectra and pion interferometry data, $\epsilon_0 = 430$ GeV/fm^3 and $\alpha = 0.45$ fm (the maximal initial transverse velocity at the very periphery of the system is then 0.05).

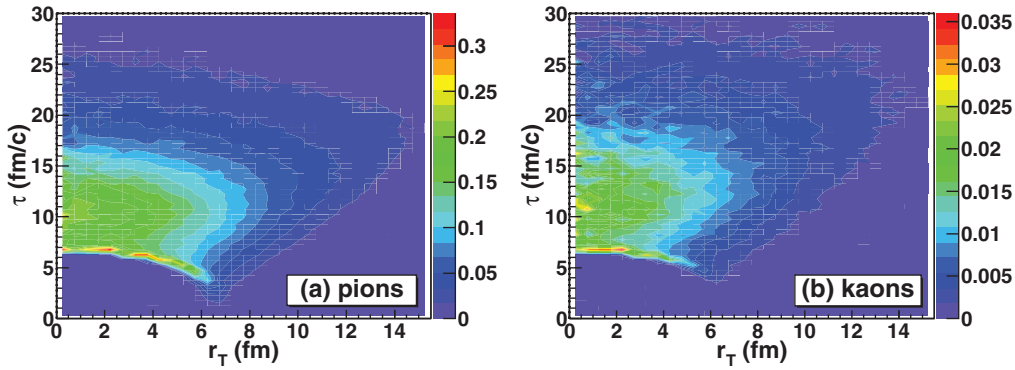

FIG. 1. (Color online) The angle-averaged emission functions $p^0\tau\langle g(x,p)\rangle_\phi$ (fm^{-3} GeV^{-2}) for pions (a) and kaons (b) from HKM simulations of Au + Au collisions at the top RHIC energy, $0.2 < p_T < 0.36$ GeV/c, $|y| < 0.35$, $c = 0\%$–20%.

It is worth noting that we are not planning to analyze and demonstrate how much worse will be results with other initial conditions. Our viewpoint is as follows. During the 1990s and 2000s great efforts were made to clarify a spatiotemporal structure of particle emission within hydrodynamics-inspired parametrizations based on the Cooper-Frye prescription, e.g., the "blast-wave" parametrization. This trend has not brought convincing success in a complex description of different observables; moreover, it collides with principal problems. It is clear now that the emission structure should be analyzed within a continuous emission of particles in dynamical evolutionary models, which are still quite different. One of our tasks is to restore the full emission function which describes simultaneously spectra, their azimuthal asymmetry, Gaussian fits for the Bose-Einstein correlation functions, the non-Gaussian source functions, etc. In case of success, no matter how advanced future models will be, they will have a reference point: the spatiotemporal structure of an emission function that describes the experiment well.

In Fig. 1 we demonstrate plots of pion and kaon angle-averaged emission functions $p^0\tau\langle g(x,p)\rangle_\phi$ for $0.2 < p_T < 0.36$ GeV/c, calculated in HKM at the selected initial conditions described above for the top RHIC energy.

The source functions are calculated from the event-generator output according to the formula

$$S(\mathbf{r}^*) = \frac{\sum_{i\neq j}\delta_\Delta(\mathbf{r}^* - \mathbf{r}_i^* + \mathbf{r}_j^*)}{\sum_{i\neq j} 1}. \tag{21}$$

Here $\mathbf{r}_i^*$ and $\mathbf{r}_j^*$ are the particles' space positions, and $\mathbf{r}^*$ is the particles' separation in the pair rest frame, $\delta_\Delta(x) = 1$ if $|x| < \Delta r/2$ and 0 otherwise, and Δr is the size of the histogram bin. The results of the calculation depend weakly on the histogram bin size (increasing the bin size twice leads to an increase of the extracted source radius of ∼1.5% and does not noticeably affect the heavy tail shape). In this paper we chose the bin size to be the same as in the experimental plots from [17].

In the PHENIX experiment [17] the measured correlation function is decomposed into Cartesian correlation moments,

$$R(\mathbf{q}) = \sum_l \sum_{\alpha_1\cdots\alpha_l} R^l_{\alpha_1\cdots\alpha_l}(q)\, A^l_{\alpha_1\cdots\alpha_l}(\Omega_\mathbf{q}), \tag{22}$$

where $l = 0, 1, 2, \ldots$, $\alpha_i = x$, y or z, $A^l_{\alpha_1\cdots\alpha_l}(\Omega_\mathbf{q})$ are Cartesian harmonic basis elements ($\Omega_\mathbf{q}$ is the solid angle in $\mathbf{q}$ space), and $R^l_{\alpha_1\cdots\alpha_l}(q)$ are Cartesian correlation moments given by

$$R^l_{\alpha_1\cdots\alpha_l}(q) = \frac{(2l+1)!!}{l!}\int \frac{d\Omega_\mathbf{q}}{4\pi} A^l_{\alpha_1\cdots\alpha_l}(\Omega_\mathbf{q})\, R(\mathbf{q}). \tag{23}$$

The obtained correlation moments then are used as the input data for the source imaging method. In [17] only the even moments up to order $l = 6$ were utilized, whereas the odd moments were found to be consistent with zero, as was

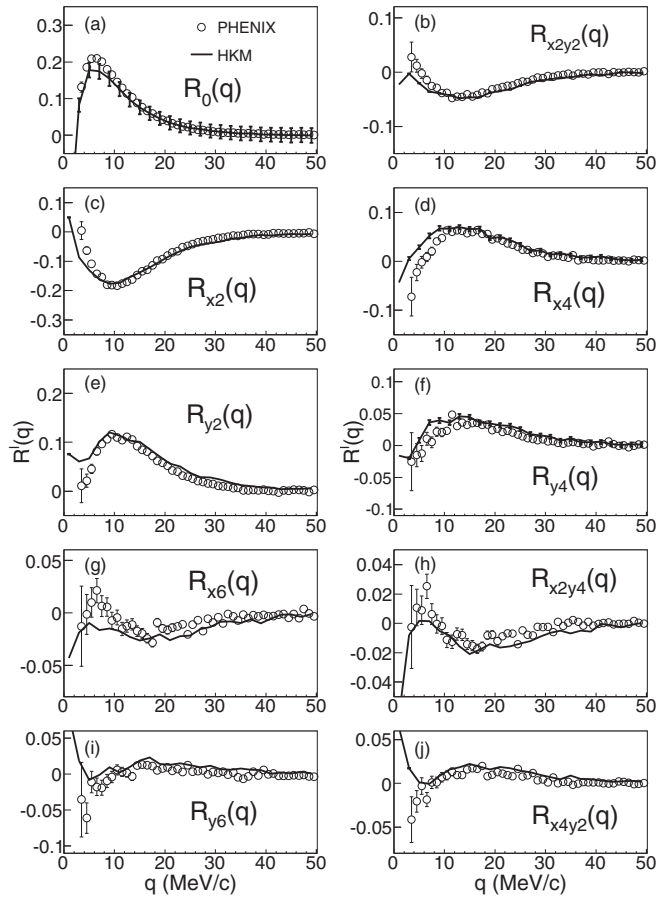

FIG. 2. Two-pion correlation moments $R_{xl_x yl_y}(q)$ obtained from the HKM model (solid lines) and from the data measured by PHENIX (open circles), $0.2 < p_T < 0.36$ GeV/c, $|y| < 0.35$, $c = 0\%$–20%.

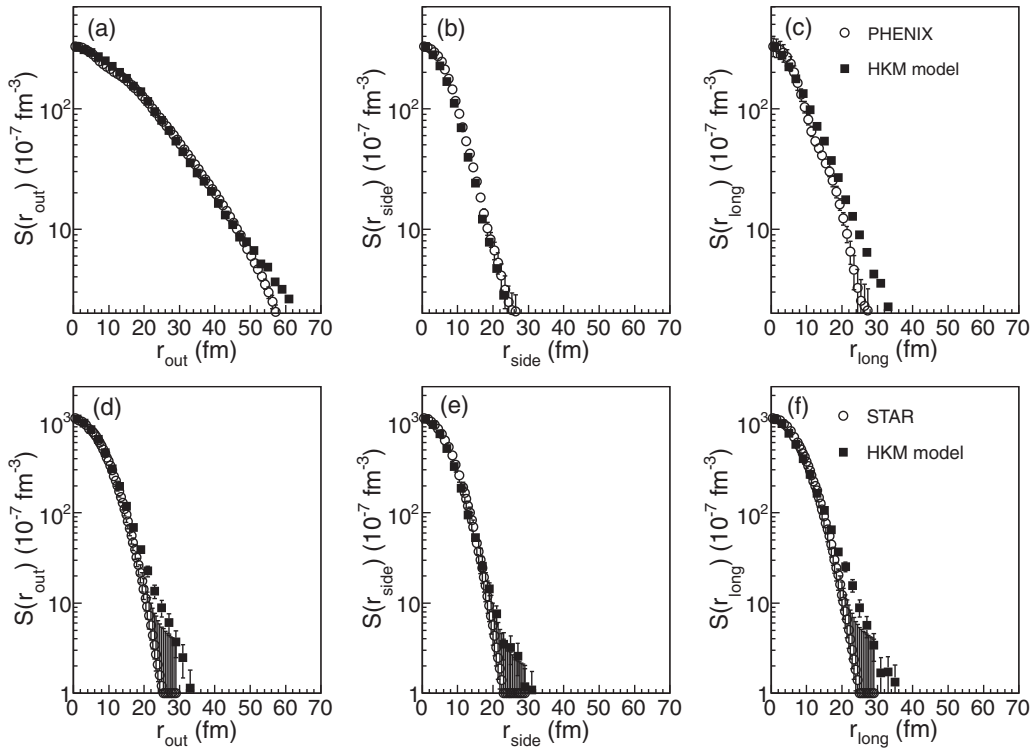

FIG. 3. Pion (top) and kaon (bottom) source function projections extracted from the HKM model compared with the ones obtained by PHENIX and STAR from the experimental correlation data using the imaging procedure, $0.2 < p_T < 0.36$ GeV/c, $|y| < 0.35$ for pions and $|y| < 0.5$ for kaons, $c = 0\%$–20%.

expected from symmetry considerations, and the moments of higher order were found to be negligible.

To demonstrate the model's reliability in describing the experimental data we compare in Fig. 2 the simulated two-pion Cartesian correlation moments with the experimental ones. Among all the moments used in the correlation function decomposition only ten moments presented in the figure are independent, and the rest can be expressed through these ten. Here $R_{xl_xyl_y}$ denotes the Cartesian correlation moment corresponding to $l = l_x + l_y$, $\alpha_1 = \cdots = \alpha_{l_x} = x$, and $\alpha_{l_x+1} = \cdots = \alpha_l = y$. As one can see, the HKM calculation result is in a good agreement with the experiment.

The comparison of projections of the three-dimensional pion and kaon source functions calculated in HKM with the PHENIX and STAR experimental data can be found in Fig. 3.[3] Here the out-side-long coordinate system is used, where the *out* axis is directed along the pair total momentum, the *long* direction coincides with the beam axis, and the *side* axis is perpendicular to the latter two ones.

We can see that the source functions are reasonably well reproduced by HKM both for pions and kaons, including the non-Gaussian tails in the *out* and *long* directions for the pion case. The range of the $S(r_{\rm long})$ projection reflects the source lifetime, and $S(r_{\rm out})$ is affected by several factors. Since the *out* direction corresponds to the pair momentum in a longitudinally comoving system (LCMS), the tail in $S(r_{\rm out})$ can be partially explained by the Lorentz dilation at boost from the LCMS to the pair center-of-mass system (PCMS). However, the estimates made in [44] show that, even at the maximal Lorentz dilation, when the $R_{\rm out}$ value in the PCMS is γ times larger than the LCMS one, the observed long-range source component cannot be explained only by such a kinematic transformation. Another possible explanation consists of associating the long-range tail with long delays between particle emission times due to a halo of secondary particles from long-lived resonance decays and due to hadron rescatterings. The latter may cause under certain conditions the so-called anomalous diffusion of particles, characterized by an increasing-in-time mean free path [45].

Let us investigate the role of secondary particles from the long-lived resonances decays and particle rescatterings in the formation of the observed heavy tail. In Fig. 4 we present the different projections of three uniformly normalized source functions, constructed from different model outputs (open markers): the full one, the model output with rescatterings turned off, and the one containing only primary particles emitted at the hadronization hypersurface, i.e., with both

[3]The demonstrated HKM source functions (as well as the correlation moments in the Fig. 2) are scaled by a factor $\lambda_{\rm exp}/\lambda_{\rm HKM} < 1$, which is the ratio of the experimental $\lambda_{\rm exp}$ and the model $\lambda_{\rm HKM}$ correlation function suppression parameters, which define also the source function intercept. In the present study we do not aim to analyze in detail the reasons for disagreement between both λ values (the smaller $\lambda_{\rm exp}$ value could be caused by, e.g., misidentification of a certain fraction of particles in the experiment, etc.). Instead we would like to focus on exploring the space-time extent of the source, reflected in the *shape* of the source function, which is reproduced well in our simulations as one can see.

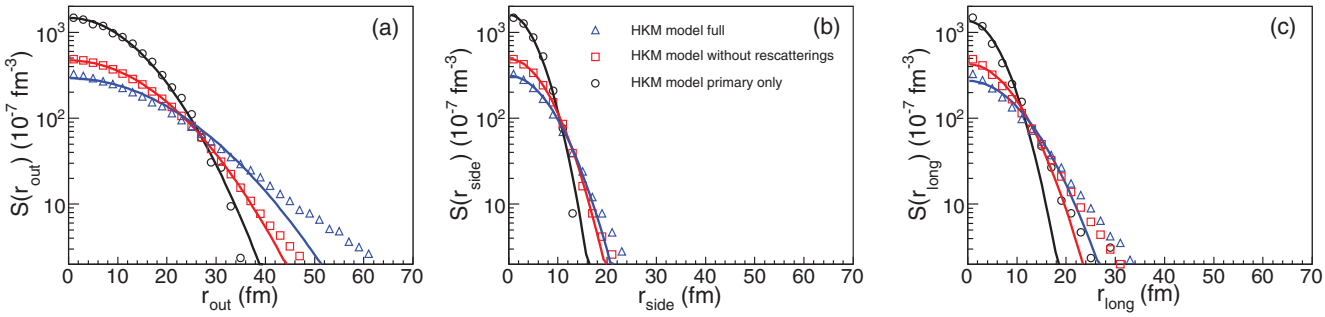

FIG. 4. (Color online) The different projections of uniformly normalized HKM pion source functions constructed from the full model output (triangles), model output without rescatterings (rectangles), and the primary particles only (circles), $0.2 < p_T < 0.36$ GeV/c, $|y| < 0.35$. Solid lines correspond to the Gaussian fits to corresponding HKM results.

rescatterings and resonances decays turned off. Along with the model data we also show the corresponding Gaussian fits (solid lines). Considering the *out*-direction profile, one can see that the full model output has a large non-Gaussian tail, while in the case of no rescatterings it is quite reduced. The primary particles' source function is almost Gaussian in the transverse direction. It seems that the exclusion of rescatterings reduces the *out* tail more significantly than the exclusion of the resonance decay contribution, so the rescatterings seem to play the main role in the tail formation. Also one can conclude that the role of the Lorentz boost to the PCMS should be of minor importance, since the tail is already practically absent for the source function built from primary particles in the PCMS, so that accounting for the Lorentz transformation can only change the Gaussian interferometry radius $R_{\rm out}$, but cannot additionally reduce the $S(r_{\rm out})$ deviation from Gaussian form by any noticeable extent.

The reason for a slight *out* and *long* tails overestimation obtained in HKM as compared to the experiment is not completely clear at the moment. To some extent it could be possibly explained by the peculiarities of rescattering treatment for resonances in the UrQMD hadronic cascade. However, most probably it is mainly connected with the substance of the experimental imaging procedure, described in the Sec. II. In the experiment one does not measure the source function itself, but restores it from the measured correlation function. The latter is typically suppressed due to the misidentification problem and due to the particles coming from long-lived resonance decays, which contribute to the single-particle spectrum, but are almost imperceptible

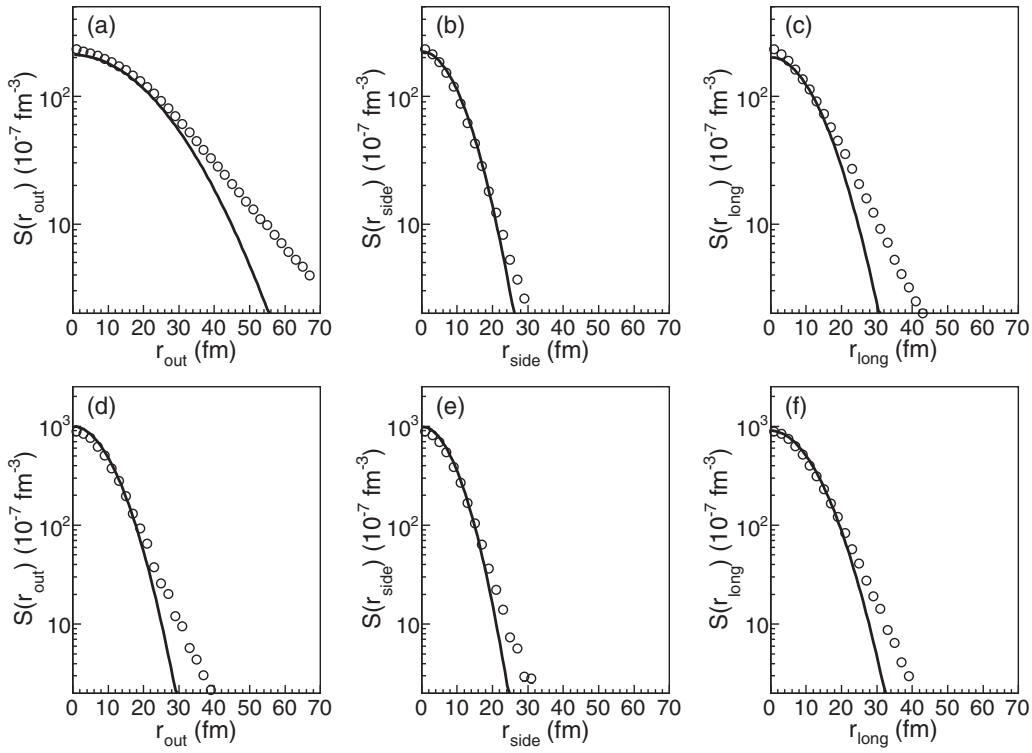

FIG. 5. Pion (top row) and kaon (bottom row) source function projections from HKM with parameters adjusted for Pb + Pb LHC collisions at $\sqrt{s_{NN}} = 2.76$ TeV, $c = 0\%$–5%, $0.2 < p_T < 0.36$ GeV/c, $|y| < 0.5$. Solid lines represent the Gaussian fits to the corresponding HKM calculations, presented by circles.

in two-particle spectrum measurement. Hence, the source function, restored from such a suppressed correlation function, should have a smaller tail as compared to the actual one. In our calculations we build the source function directly from the event-generator output. In such a way we do not face the above-mentioned problems arising in the experiment, and thus we should obtain a more realistic, higher tail in the source function.

As for interpreting the observed tails as the signals of the phase transition, the situation is not so easy. Different criteria for detecting the transition occurrence were proposed, such as the Bertsch criterion $R_{\rm out}/R_{\rm side} \gg 1$ or the large $R_{\rm long}$ criterion. However, in practice there exist certain difficulties in their application. For example, if the matter expansion starts from a state of pure phase and then at some stage of the evolution the system undergoes a phase transition, fast matter expansion will continue out of inertia, and we will not find the transition signs in the measured data. To see these signs, one would have to create such initial conditions for matter evolution that it would start from a transient state where different phases exist simultaneously. Apart from this, the application of the Bertsch criterion is troubled by the likely existence of a positive $r_{\rm out}$–t correlation in the sectors of the freeze-out hypersurface, where the particles are emitted from a surface of the hydrodynamic tube, that causes the negative sign of the space-time correlation contribution to $R_{\rm out}$ and in such a way reduces the observed $R_{\rm out}$ value [46,47]:

$$R^2_{\rm out}(p) = \langle(\Delta r_{\rm out} - v_{\rm out}\Delta t)^2\rangle_p = \left\langle \Delta r^2_{\rm out}\right\rangle_p + v^2_{\rm out}\langle\Delta t^2\rangle_p - 2v_{\rm out}\langle\Delta r_{\rm out}\Delta t\rangle_p. \quad (24)$$

This means that the observed $R_{\rm out}/R_{\rm side} \approx 1$ ratio does not necessarily indicate a short emission duration. However, one can try to extract the mean emission duration as well as the system's lifetime from the event-generator calculations.

In [17] the experimental data for pions are presented together with results of simulations in the THERMINATOR event generator with blast-wave parametrization for the freeze-out hypersurface, $\tau = \tau_0 + a\rho$, where τ_0 is the source proper breakup time, ρ is the transverse radial coordinate, $\rho \leqslant \rho_{\rm max}$, and a is a free parameter describing space-time correlations. The simulations give the best data description when the resonances decays are turned on and particle emission is supposed to take place from the family of hypersurfaces defined by different breakup proper times τ_0', distributed according to exponential law, $\frac{dN}{d\tau_0'} = \frac{\Theta(\tau_0'-\tau_0)}{\Delta\tau}\exp(\frac{\tau_0'-\tau_0}{\Delta\tau})$. The width $\Delta\tau$ is interpreted then as the mean emission duration time in the rest frame.[4]

The break-up proper time $\tau_0 \sim 9$ fm/c and small but nonzero proper emission duration in the rest frame $\Delta\tau \sim 2$ fm/c, for which simulation results are closest to the data, appear to be incompatible with the first-order transition scenario [48,49], but can point to a crossover phase transition [19]. Finite emission duration in the used parametrization (and, partly, the resonance decays contribution) leads to a quite appreciable pion emission time differences in the LCMS, with $\langle|\Delta t_{\rm LCMS}|\rangle \approx 12$ fm/c.

As for the hybrid HKM, the crossover phase transition is assumed in the model from the beginning in the equation of state for the hydrodynamics stage. We use the isotherm $T_{\rm ch}$ as the single freeze-out hypersurface, which in the case of top RHIC energies spreads in proper time up to $\tau_{\rm max} \approx 7$ fm/c, and the mean LCMS emission time difference for pions in our calculations is $\langle|\Delta t_{\rm LCMS}|\rangle = 13$ fm/c including emission from resonances and after rescatterings, which is apparently in accordance with the results obtained within the THERMINATOR parametrization.

Finally, in Figs. 5 and 6 we show our predictions concerning source function and Cartesian correlation moments $R_{xl_x yl_y}(q)$ for the case of 5% most central LHC Pb + Pb collisions at the energy $\sqrt{s_{NN}} = 2.76$ TeV. For these calculations we take the same $\alpha = 0.45$ fm as for the RHIC case, and the maximal energy density at starting time $\tau = 0.1$ fm/c is equal to $\epsilon = 1300$ GeV/fm^3. In contrast to the RHIC case, these LHC source functions and correlation moments are demonstrated as is, not scaled by the factor $\lambda_{\rm exp}/\lambda_{\rm HKM}$. We see that, according to our calculations, the kaon source functions at LHC also have to be closer to Gaussian shape, whereas for the pion case

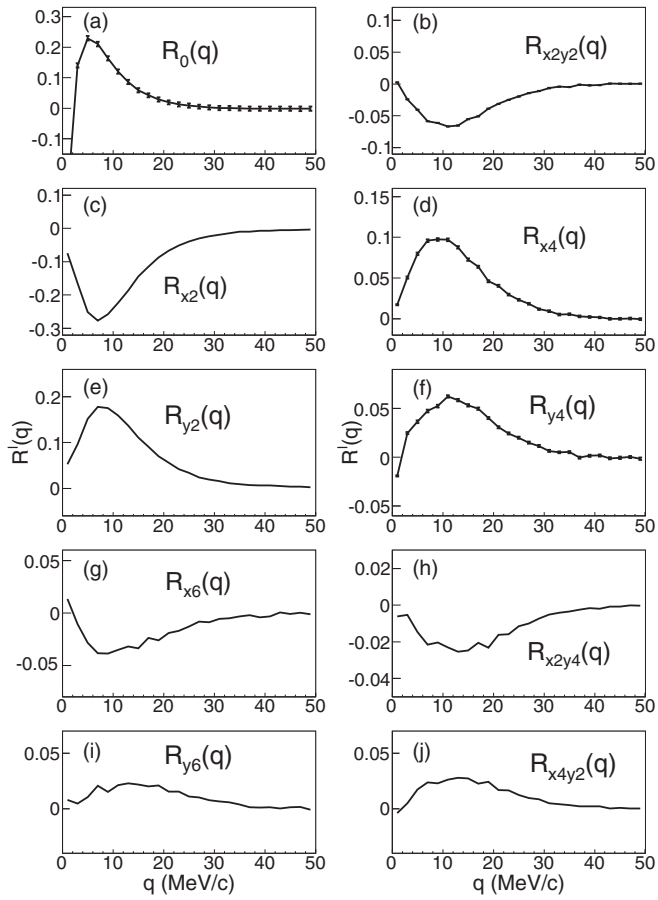

FIG. 6. Pion Cartesian correlation moments $R_{xl_x yl_y}(q)$ from the HKM with parameters adjusted for Pb + Pb LHC collisions at $\sqrt{s_{NN}} = 2.76$ TeV, $c = 0\%$–5%, $0.2 < p_T < 0.36$ GeV/c, $|y| < 0.5$.

[4]One can say that such a parametrization efficiently accounts for particle rescatterings, which are not implemented in THERMINATOR, but seem to strongly influence the measured source function.

the source function should have a heavy tail. Also the source functions for the case of LHC energy are wider than the ones for the RHIC case that corresponds to the larger homogeneity lengths in the LHC case, a more prolonged rescattering stage, and so prolonged particle emission as is expected at increasing collision energy.

IV. CONCLUSIONS

In this paper we considered the analysis of heavy ion collision space-time structure in terms of emission source functions, or a time-integrated particle-emission-points separation distribution related to the pair rest frames. Experimental source functions serve as model-independent characteristics of the size and shape of the emission region, separated from the particle interaction effects. Restored from the measured correlation functions with a sophisticated source imaging technique, experimental source functions can be compared with the model ones, directly extracted from the event generators of a particular model.

We presented the results of pion and kaon source function simulations within the hydrokinetic model (HKM) for semicentral Au + Au collisions at top RHIC energy $\sqrt{s_{NN}} =$ 200 GeV together with the predictions for the central LHC Pb + Pb collisions at $\sqrt{s_{NN}} = 2.76$ TeV. The results for RHIC are in good agreement with the experimental data.

The long-range power-law tail in the pair momentum direction, observed in pion source functions, can be explained by the combined influence of secondary particles coming from the long-lived resonance decays and particle rescatterings, whose contribution seems to be dominating. The role of the kinematic transformation to the pair rest frame seems to be of minor importance. The model calculations also point to substantial emission time differences for pion pairs that should take place in the experiment.

We also demonstrate the spatio-temporal structure of pion and kaon emission (Fig. 1), with which one can simultaneously well describe not only the observed spectra, elliptic flow, and Gaussian interferometry radii, but also detailed emission characteristics, such as the non-Gaussian source functions.

The behavior of the predicted source functions for the LHC case is qualitatively similar to the RHIC one, including the presence of heavy tails for pions and an almost Gaussian source shape for kaons. Quantitatively, the LHC source functions are wider than the ones at RHIC, indicating larger homogeneity lengths and a prolonged particle rescattering stage.

ACKNOWLEDGMENTS

The authors are grateful to M. Sumbera and P. Chung for fruitful discussions. The research was carried out within the scope of the EUREA, European Ultra Relativistic Energies Agreement (European Research Group “Heavy ions at ultrarelativistic energies”), and is supported by the National Academy of Sciences of Ukraine (Agreement No. F4-2013) and by the State Fund for Fundamental Researches of Ukraine (Agreement No. F33/24-2013). The work was supported by the Program of Fundamental Research of the Department of Physics and Astronomy of the NAS of Ukraine.

[1] G. Goldhaber, S. Goldhaber, W. Lee, and A. Pais, Phys. Rev. **120**, 300 (1960).
[2] G. I. Kopylov and M. I. Podgoretsky, Sov. J. Nucl. Phys. **15**, 219 (1972); **18**, 336 (1974); **19**, 215 (1974).
[3] G. Cocconi, Phys. Lett. B **49**, 459 (1974).
[4] Yu. M. Sinyukov, R. Lednický, S. V. Akkelin, J. Pluta, and B. Erazmus, Phys. Lett. B **432**, 248 (1998).
[5] Yu. M. Sinyukov and V. M. Shapoval, Phys. Rev. D **87**, 094024 (2013).
[6] Yu. M. Sinyukov, Nucl. Phys. A **566**, 589 (1994); in *Hot Hadronic Matter: Theory and Experiment*, edited by J. Letessier, H. H. Gutbrod, and J. Rafelski (Plenum, New York, 1995), p. 309.
[7] S. V. Akkelin and Yu. M. Sinyukov, Phys. Lett. B **356**, 525 (1995).
[8] D. A. Brown and P. Danielewicz, Phys. Lett. B **398**, 252 (1997).
[9] D. A. Brown and P. Danielewicz, Phys. Rev. C **57**, 2474 (1998).
[10] D. A. Brown and P. Danielewicz, Phys. Rev. C **64**, 014902 (2001).
[11] J. P. Sullivan *et al.*, Phys. Rev. Lett. **70**, 3000 (1993).
[12] S. Nickerson, T. Csörgő, and D. Kiang, Phys. Rev. C **57**, 3251 (1998).
[13] T. Csörgö, B. Lörstad, J. Schmidt-Sørensen, and A. Ster, Eur. Phys. J. C **9**, 275 (1999).
[14] S. Pratt, T. Csörgő, and J. Zimányi, Phys. Rev. C **42**, 2646 (1990).
[15] S. Y. Panitkin and D. A. Brown, Phys. Rev. C **61**, 021901(R) (1999).
[16] B. Andersson and W. Hofmann, Phys. Lett. B **169**, 364 (1986).
[17] S. Afanasiev *et al.* (PHENIX Collaboration), Phys. Rev. Lett. **100**, 232301 (2008).
[18] P. Chung (STAR Collaboration), PEPAN Lett. A **8**, 219 (2011), arXiv:1012.5674; L. Adamczyk *et al.* (STAR Collaboration), Phys. Rev. C **88**, 034906 (2013), arXiv:1302.3168.
[19] R. A. Lacey, Braz. J. Phys. **37**, 893 (2007); **35**, 104139 (2008).
[20] A. Kisiel, T. Taluc, W. Broniowski, and W. Florkowski, Comput. Phys. Commun. **174**, 669 (2006).
[21] T. J. Humanic, Nucl. Phys. A **715**, 641c (2003); Phys. Rev. C **73**, 054902 (2006).
[22] R. Lednický and V. L. Lyuboshitz, Yad. Fiz. **35**, 1316 (1981) [Sov. J. Nucl. Phys. **35**, 770 (1982)]; in *Proceedings of the International Workshop on Particle Correlations and Interferometry in Nuclear Collisions (CORINNE 90), Nantes, France, 1990*, edited by D. Ardouin (World Scientific, Singapore, 1990), pp. 42–54.
[23] J. Adams *et al.* (STAR Collaboration), Phys. Rev. C **74**, 064906 (2006).
[24] P. J. Siemens and J. O. Rasmussen, Phys. Rev. Lett. **42**, 880 (1979); E. Schnedermann, J. Sollfrank, and U. Heinz, Phys. Rev. C **48**, 2462 (1993); A. Kisiel, Braz. J. Phys. **37**, 917 (2007).
[25] Yu. M. Sinyukov, S. V. Akkelin, and Y. Hama, Phys. Rev. Lett. **89**, 052301 (2002).

[26] S. V. Akkelin, Y. Hama, Iu. A. Karpenko, and Yu. M. Sinyukov, Phys. Rev. C **78**, 034906 (2008).
[27] Iu. A. Karpenko and Yu. M. Sinyukov, Phys. Rev. C **81**, 054903 (2010).
[28] Iu. A. Karpenko, Yu. M. Sinyukov, and K. Werner, Phys. Rev. C **87**, 024914 (2013).
[29] S. V. Akkelin and Yu. M. Sinyukov, Phys. Rev. C **73**, 034908 (2006).
[30] S. R. de Groot, W. A. van Leeuwen, and Ch. G. van Weert, *Relativistic Kinetic Theory* (North-Holland, Amsterdam, 1980).
[31] R. Lednický, Phys. Part. Nucl. **40**, 307 (2009).
[32] E. Fermi, Z. Phys. **88**, 161 (1934); translated in F. L. Wilson, Am. J. Phys. **36**, 1150 (1968).
[33] S. E. Koonin, Phys. Lett. B **70**, 43 (1977).
[34] M. Gyulassy, S. K. Kauffmann, and L. W. Wilson, Phys. Rev. C **20**, 2267 (1979).
[35] R. Lednický, V. V. Lyuboshitz, and V. L. Lyuboshitz, Phys. At. Nucl. **61**, 2050 (1998); R. Lednický, J. Phys. G: Nucl. Part. Phys. **35**, 125109 (2008).
[36] R. Lednický, Phys. Part. Nucl. Lett. **8**, 965 (2011).
[37] D. A. Brown, A. Enokizono, M. Heffner, R. Soltz, P. Danielewicz, and S. Pratt, Phys. Rev. C **72**, 054902 (2005).
[38] R. Lednický, V. L. Lyuboshitz, B. Erazmus, and D. Nouais, Phys. Lett. B **373**, 30 (1996).
[39] P. Danielewicz and S. Pratt, Phys. Rev. C **75**, 034907 (2007).
[40] Z. Chajecki and M. Lisa, Braz. J. Phys. **37**, 1057 (2007).
[41] M. Laine and Y. Schroder, Phys. Rev. D **73**, 085009 (2006).
[42] F. Cooper and G. Frye, Phys. Rev. D **10**, 186 (1974).
[43] W. Broniowski, M. Rybczynski, and P. Bozek, Comput. Phys. Commun. **180**, 69 (2009), arXiv:0710.5731v3.
[44] S. S. Adler *et al*. (PHENIX Collaboration), Phys. Rev. Lett. **98**, 132301 (2007).
[45] M. Csanad, T. Csörgő, and M. Nagy, Braz. J. Phys. **37**, 1002 (2007).
[46] M. S. Borysova, Yu. M. Sinyukov, S. V. Akkelin, B. Erazmus, and Iu. A. Karpenko, Phys. Rev. C **73**, 024903 (2006).
[47] Iu. A. Karpenko and Yu. M. Sinyukov, Phys. Lett. B **688**, 50 (2010).
[48] S. Pratt, Phys. Rev. Lett. **53**, 1219 (1984).
[49] D. H. Rischke *et al*., Nucl. Phys. A **608**, 479 (1996).